

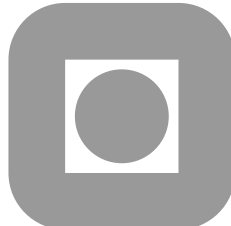
NORGES TEKNISK-NATURVITENSKAPELIGE
UNIVERSITET

**Semi-Lagrangian exponential integrators for the
incompressible Navier-Stokes equations**

by

Elena Celledoni, Bawfeh Kingsley Kometa and Olivier Verdier

PREPRINT
NUMERICS NO. 7/2011



NORWEGIAN UNIVERSITY OF
SCIENCE AND TECHNOLOGY
TRONDHEIM, NORWAY

This report has URL

<http://www.math.ntnu.no/preprint/numerics/2011/N7-2011.pdf>

Address: Department of Mathematical Sciences, Norwegian University of Science and
Technology, N-7491 Trondheim, Norway.

Semi-Lagrangian exponential integrators for the incompressible Navier-Stokes equations

Elena Celledoni, Bawfeh Kingsley Kometa and Olivier Verdier

September 14, 2011

Direct applications of high order DIRK-CF methods as presented in [7] to the incompressible Navier- Stokes equations were found to yield a loss in order of convergence. The DIRK-CF methods are exponential integrators arising from the IMEX Runge-Kutta techniques proposed in [1], and are semi-Lagrangian when applied to convection diffusion equations. As discussed in [17], inappropriate implementation of projection methods for incompressible flows can lead to a loss in the order of convergence. In this paper we recover the full order of the IMEX methods using projections onto the space of divergence-free vector fields and we discuss the difficulties encountered in using similar techniques for the semi-Lagrangian DIRK-CF methods. We finally assess the performance of the semi-Lagrangian DIRK-CF methods for the Navier-Stokes equations in convection dominated problems.

1 Introduction

Consider the incompressible Navier-Stokes equations

$$\mathbf{u}_t + \mathbf{u} \cdot \nabla \mathbf{u} = \nu \nabla^2 \mathbf{u} - \nabla p \quad (1.1)$$

$$\nabla \cdot \mathbf{u} = 0, \quad (1.2)$$

$$\mathbf{u}|_{\partial\Omega} = 0, \quad (1.3)$$

here $\mathbf{u} = \mathbf{u}(\mathbf{x}, t)$ on the cylinder $\Omega \times [0, T]$ is the velocity filed ($\Omega \subset \mathbf{R}^d$ and $d = 2, 3$), subjected to the incompressibility constraint (1.2), $p = p(\mathbf{x}, t)$ is the pressure and plays the role of a Lagrange multiplier, and ν is the kinematic viscosity of the fluid. We consider no slip or periodic boundary conditions

$$\mathbf{u}|_{\partial\Omega} = \mathbf{u}_b, \quad (1.4)$$

$$\mathbf{u} \text{ periodic.} \quad (1.5)$$

In the case of no slip boundary conditions we will also use that $\mathbf{u}_b \cdot \mathbf{n} = 0$ where \mathbf{n} is the unit normal to the boundary $\partial\Omega$. For no slip boundary conditions we will mostly consider the case

$$\mathbf{u}_b = 0. \quad (1.6)$$

The variables (\mathbf{u}, p) are sometimes called primitive variables and the accurate approximation of both these variables is desirable in numerical simulations.

In this paper we study semi-Lagrangian discretization methods in time to be used in combination with high order spatial discretizations of the Navier-Stokes equations, like for example spectral element methods. High order methods are particularly interesting in cases when highly accurate numerical approximations of a given flow case are required. A relevant situation is the direct numerical simulation of turbulence phenomena (DNS), as pointed out for example in [23].

The methods we consider here are implicit-explicit methods of Runge-Kutta type which we named DIRK-CF, and they have been proposed in [6, 7]. These methods arise from IMEX techniques proposed in [2, 1]. In addition to being implicit-explicit the methods are semi-Lagrangian and they show improved performance in convection dominated problems. So far the case of linear and nonlinear convection diffusion equations have been considered.

It is our goal in this paper to further investigate the extension of these methods to the incompressible Navier-Stokes equations and to assess their performance. Given a time-stepping technique, a very used approach to adapt the method to the incompressible Navier-Stokes equations is by means of projections. The primary example of this technique, and most famous projection method for the incompressible Navier-Stokes equations is the Chorin's projection method, proposed by Chorin in [9, 10] and Témam [22]. Chorin's method is a version of the implicit Euler integration method adapted to the Navier-Stokes equations.

The study of the temporal order of this method was considered in [20, 21] and it revealed order one for the velocity and only $\frac{1}{2}$ for the approximation of the pressure. This and similar order reduction phenomena are typical of projection methods for Navier-Stokes equations and must be handled properly to achieve higher order. Lately a better understanding of the issues of order reduction in a variety of projection methods, and remedies to this problem appeared in [19, 3, 17].

We consider projection methods for IMEX Runge-Kutta schemes as a starting point to discuss the extension of the methods of [7] to the Navier-Stokes equations. In this preliminary work we explain some of the difficulties encountered in the case of the semi-Lagrangian methods, spectral element space discretizations and the Navier-Stokes equations. We obtain methods of IMEX type which show up to third order temporal accuracy in the velocity and first order in the pressure. The semi-Lagrangian methods achieve up to second temporal order in the velocity.

In section 2 we consider appropriate projections to be used in the reformulation of our methods in the context of Navier-Stokes equations, including some relevant background material. In section 3 we discuss implicit-explicit methods, and the semi-Lagrangian methods named DIRK-CF and their extensions to Navier-Stokes equations. Section 4 is devoted to numerical experiments. In this section we provide numerical verification of the temporal order of the methods; we illustrate the benefits of the proposed semi-Lagrangian methods in the case of convection dominated problems; we also devote this section to the description of the implementation details behind our numerical results.

2 Projection methods for the incompressible Navier-Sokes equations

2.1 Leray projector

According to the Helmholtz decomposition of vector fields, $\mathbf{w} \in (L^2(\mathbf{R}^d))^d$ can be decomposed into a curl-free and a divergence-free part:

$$\mathbf{w} = \nabla\phi + \mathbf{v}, \quad \nabla \cdot \mathbf{v} = 0. \quad (2.1)$$

We are interested in such decomposition on bounded domains Ω , taking into account boundary conditions. We consider a projection on the subset of the space of divergence free vector fields, with prescribed boundary conditions on $\partial\Omega$:

$$H = \{\mathbf{v} \in (L^2(\Omega, \mathbf{R}^d))^d \mid \nabla \cdot \mathbf{v} = 0, \mathbf{v}|_{\partial\Omega} = \text{bc}\}, \quad \mathcal{P} : \mathcal{W} \subset (L^2(\Omega, \mathbf{R}^d))^d \rightarrow H,$$

and $\mathcal{W} \subset (L^2(\Omega, \mathbf{R}^d))^d$ an appropriate subset of $(L^2(\Omega, \mathbf{R}^d))^d$, here the boundary conditions (bc) are either periodic or $\mathbf{n} \cdot \mathbf{v}|_{\partial\Omega} = 0$.

So \mathcal{P} is such that

$$\mathcal{P}(\mathbf{w}) = \mathbf{v}, \quad (2.2)$$

satisfying the conditions

$$\nabla \cdot \mathbf{v} = 0, \quad \mathbf{v}|_{\partial\Omega} = \text{bc}. \quad (2.3)$$

Assuming \mathbf{w} satisfies boundary conditions compatible with \mathbf{v} (say \mathbf{w} periodic or with no slip boundary conditions), we can take \mathcal{P} to be the Leray projector [14]. This projector is constructed by taking \mathbf{v} as

$$\mathcal{P}(\mathbf{w}) = \mathbf{v} = \mathbf{w} - \nabla\phi,$$

where ϕ is the solution of the Poisson equation

$$\nabla^2\phi = \nabla \cdot \mathbf{w} \quad (2.4)$$

and boundary conditions for ϕ either periodic or Neumann:

$$0 = \mathbf{n} \cdot \mathbf{v}|_{\partial\Omega} = \mathbf{n} \cdot \mathbf{w}|_{\partial\Omega} - \mathbf{n} \cdot \nabla\phi|_{\partial\Omega}. \quad (2.5)$$

2.2 Incompressible Navier-Stokes and projections

In general, taking the divergence of the momentum equation, (1.1), we obtain a Poisson equation for the pressure

$$\nabla^2 p = \nabla \cdot (\nu \Delta \mathbf{u} - \mathbf{u} \cdot \nabla \mathbf{u}). \quad (2.6)$$

When \mathbf{u} is space-periodic, i.e. (1.5), the pressure p is fully defined in terms of the velocity field \mathbf{u} and the periodicity condition. In the case of no slip boundary conditions, (1.4) and (1.6), solving the Poisson equation for p by imposing

$$\frac{\partial p}{\partial \mathbf{n}} = \nu \Delta \mathbf{u} \cdot \mathbf{n},$$

on the boundary, fully determines the pressure. In both cases we can write $p = \psi(\mathbf{u})$, [14]. We can then eliminate the pressure from the momentum equation and obtain

$$\mathbf{u}_t - \nu \Delta \mathbf{u} + \mathbf{u} \cdot \nabla \mathbf{u} + \nabla p = \mathbf{u}_t - \nu \Delta \mathbf{u} + \mathbf{u} \cdot \nabla \mathbf{u} + \nabla \psi(\mathbf{u}) = 0.$$

We observe that for \mathbf{u} satisfying the Navier-Stokes equations (1.1-1.3) we have

$$\mathcal{P}(\mathbf{u}) = \mathbf{u}, \quad \mathcal{P}(\mathbf{u}_t) = \mathbf{u}_t, \quad \mathcal{P}(\nabla p) = 0,$$

and we can rewrite the Navier-Stokes equations as

$$\mathbf{u}_t = \mathcal{P}(\nu \Delta \mathbf{u} - \mathbf{u} \cdot \nabla \mathbf{u} - \nabla p). \quad (2.7)$$

An alternative formulation [14] is

$$\mathbf{u}_t = \nu \mathcal{P}(\Delta \mathbf{u}) - \mathcal{P}(\mathbf{u} \cdot \nabla \mathbf{u}), \quad (2.8)$$

where the two projections correspond to two different Poisson problems which have both periodic or Neumann boundary conditions to be imposed on corresponding Lagrangian multipliers.

In the context of IMEX and semi-Lagrangian Runge-Kutta time integration methods, the formulation (2.8) seems to be the most appropriate. The intention is to apply different Runge-Kutta coefficients to the convection operator and the diffusion operator. However non-trivial complications arise when discretizing in space.

After spatial discretizations of type spectral-Galerkin or spectral element methods, we obtain a system of differential-algebraic equations of the type:

$$B\dot{y} = A y + C(y) y - D^T z, \quad D y = 0, \quad (2.9)$$

which should be satisfied with appropriate boundary conditions. Here A is the discrete Laplacian, B is the mass matrix, $C(y)$ is the discrete convection operator, D is the discrete divergence and D^T is the discrete gradient. The numerical solution $y \approx \mathbf{u}$ includes values pertaining to boundary nodes, and the discrete operators are sized accordingly. The intention is to impose the boundary conditions directly on the numerical approximation y . Boundary conditions are not inbuilt in (2.9) as in the case of finite differences discretizations, and are enforced by applying an operator R_b to the numerical solution.

If D is full rank, the Lagrangian multiplier z in (2.9) can be obtained by solving the linear system

$$DB^{-1}D^T z = DAy + DC(y)y, \quad (2.10)$$

but such z is not necessarily satisfying the boundary conditions satisfied by the pressure in (2.6) deduced from (1.1), and similarly \dot{y} is not satisfying the boundary conditions satisfied by \mathbf{u}_t in (1.1). Assuming Π denotes the projection on the space of discrete divergence free vector fields, regardless of boundary conditions, this gives

$$\Pi B^{-1}(Ay + C(y)y) = B^{-1}(Ay + C(y)y - D^T z) \quad (2.11)$$

and z the solution of (2.10), we can introduce the discrete analogs to (2.7) and (2.8) simply as

$$\dot{y} = \Pi B^{-1}(Ay + C(y)y),$$

and

$$\dot{y} = \Pi B^{-1}(Ay) + \Pi(C(y)y).$$

Applying Runge-Kutta methods, IMEX methods or semi-Lagrangian exponential integrators to these equations will produce approximations of \mathbf{u} which are divergence free, but do not, in general, satisfy the desired boundary conditions. Trying to enforce boundary conditions by using instead projections $\tilde{\Pi}$ mapping Ay and $C(y)y$ into the space of divergence free vector fields with appropriate boundary conditions, turns out to be ill-conditioned.

Another inconvenience coming from the type of discretizations considered in this work, is that the pressure is not defined on boundary nodes and the boundary conditions cannot be imposed on the pressure (as assumed for the solution of the Poisson equations pertaining to \mathcal{P}). The only acceptable alternative is to impose boundary conditions directly on the numerical approximations of the solution, i.e. the stage values of the Runge-Kutta method. We then obtain that the boundary conditions satisfied by \mathbf{u}_t are respected at the discrete level only for some appropriate, numerical, discrete derivatives.

In the next section we will show how this is handled successfully in the case of IMEX methods.

The relation between (1.1), (2.8) and (2.7) in terms of the corresponding Lagrangian multipliers might be important in order to obtain accurate approximations of the pressure. For example in the periodic case we get

$$\mathcal{P}(\Delta \mathbf{u}) = \Delta \mathbf{u} \Rightarrow \mathbf{u} \cdot \nabla \mathbf{u} + \nabla \psi(\mathbf{u}) = \mathcal{P}(\mathbf{u} \cdot \nabla \mathbf{u})$$

but in the no-slip case this is not so.

We however we always have

$$\mathbf{u} \cdot \nabla \mathbf{u} + \nabla \psi(\mathbf{u}) = (I - \mathcal{P})(\nu \Delta \mathbf{u}) + \mathcal{P}(\mathbf{u} \cdot \nabla \mathbf{u}),$$

here I denotes the identity operator.

3 High order implicit-explicit and semi-Lagrangian methods of Runge-Kutta type

3.1 IMEX Runge-Kutta

We consider IMEX methods with a DIRK (diagonally implicit Runge-Kutta) implicit part to be applied to the diffusion operator and an appropriate explicit part to be used for the convection operator. Applied to (1.1) the projected IMEX methods are

$$\mathbf{U}_i = \mathcal{P}(\mathbf{u}_n + \Delta t \sum_{j=1}^{i-1} (a_{i,j}(\Delta \mathbf{U}_j - \nabla P_j) - \tilde{a}_{i,j} \mathbf{U}_j \cdot \nabla \mathbf{U}_j) + \Delta t a_{i,i} \Delta \mathbf{U}_i), \quad i = 1, \dots, s$$

and P_i is the Lagrangian multiplier to be used to perform the projection \mathcal{P} . We assume both the Runge-Kutta methods with coefficients $\{a_{i,j}\}_{i,j=1,\dots,s}$ and $\{\tilde{a}_{i,j}\}_{i,j=1,\dots,s}$ respectively, are stiffly accurate, so, $\mathbf{u}_{n+1} = \mathbf{U}_s$. To obtain the fully discrete version of the methods we apply them first to the equation (2.9) and obtain:

$$BY_i = By_n + \Delta t \sum_{j=1}^{i-1} [a_{i,j}(AY_j - D^T Z_j) - \tilde{a}_{i,j}C(Y_j)Y_j] + \Delta t a_{i,i}(AY_i - D^T Z_i), \quad i = 1, \dots, s$$

with the constraint $DY_i = 0$. We next apply the operator R_b enforcing boundary conditions on Y_i , and finally we solve the following linear system for Y_i and Z_i ,

$$\begin{aligned} R_b(B - \Delta t a_{i,i}A)Y_i + \Delta t a_{i,i}R_bD^T Z_i &= R_b(By_n + \Delta t \sum_{j=1}^{i-1} [a_{i,j}(AY_j - D^T Z_j) + \tilde{a}_{i,j}C(Y_j)Y_j]) \\ DY_i &= 0. \end{aligned}$$

The solution of such linear system is obtained by a Schur-complement approach and the inversion of the discrete Helmholtz operator

$$R_b(B - \Delta t a_{i,i} A)$$

by applying a preconditioned conjugate gradient algorithm. We obtain that $y_{n+1} = Y_s$ is the approximation of the velocity field at time t_{n+1} and Z_s is the corresponding approximation of the pressure.

3.2 Semi-Lagrangian IMEX Runge-Kutta

We here consider a second order method presented in [7] in the case of convection diffusion equations. We refer to [7] for the general formulation of these methods, which are named DIRK-CF. We apply the method to (2.9), the first stage is

$$Y_1 = y_n, \quad Z_1 = 0, \quad \varphi_1 = I.$$

Defining $\varphi_2 = \exp(\Delta t \tilde{a}_{2,1} C(Y_1))$ the second stage is

$$Y_2 = \varphi_2[y_n + \Delta t a_{2,1} \varphi_1^{-1} B^{-1}(AY_1 - D^T Z_1)] + \Delta t a_{2,2} B^{-1}(AY_2 - D^T Z_2),$$

with $DY_2 = 0$. The term $D^T Z_1 = 0$. We now multiply both sides by B and apply R_b to obtain a linear system for Y_2 and Z_2 . This linear system is

$$\begin{aligned} R_b(B - \Delta t a_{2,2} A)Y_2 + \Delta t a_{2,2} R_b D^T Z_2 &= R_b B \varphi_2(y_n + \Delta t a_{2,1} B^{-1} A Y_1), \\ DY_2 &= 0. \end{aligned}$$

We interpret the $\varphi_1 w$ as the transport of w along the flow of the vector field Y_1 .

At the third stage, we define $\varphi_3 = \exp(\Delta t \tilde{a}_{3,1} C(Y_1) + \Delta t \tilde{a}_{3,2} C(Y_2))$ and write

$$Y_3 = \varphi_3[y_n + \Delta t a_{3,1} \varphi_1^{-1} B^{-1}(AY_1 - D^T Z_1) + \Delta t a_{3,2} \varphi_2^{-1} B^{-1}(AY_2 - D^T Z_2)] + \Delta t a_{3,3} B^{-1}(AY_3 - D^T Z_3),$$

with $DY_3 = 0$. After applying R_b we obtain the linear system

$$\begin{aligned} R_b(B - \Delta t a_{3,3} A)Y_3 + \Delta t a_{3,3} R_b D^T Z_3 &= R_b B \varphi_3(y_n + \Delta t a_{3,1} B^{-1} A Y_1 + \Delta t a_{3,2} \varphi_2^{-1} B^{-1}(AY_2 - D^T Z_2)), \\ DY_3 &= 0. \end{aligned}$$

We finally take $y_{n+1} = Y_3$. This approach to enforce boundary conditions for the DIRK-CF methods is the straightforward counterpart of the approach used for IMEX methods in the previous section, and leads to methods with temporal order at most 2 in the velocity. We were unable to obtain order three or more with this technique.

4 Numerical experiments

For the numerical experiments we shall employ a spectral element method (SEM) based on the standard Galerkin weak formulation as detailed out in [13]. We use a rectangular domain consisting of N_e uniform elements. The approximation is done in $\mathbb{P}_N - \mathbb{P}_{N-2}$ compatible velocity-pressure discrete spaces, i.e., keeping the time variable t fixed, in each element we approximate the velocity by a N -degree Lagrange polynomial based on Gauss-Lobatto-Legendre (GLL) nodes in each spatial coordinate, and the pressure by $(N-2)$ -degree Lagrange polynomial based on Gauss-Legendre (GL) nodes. The discrete spaces are spanned by tensor product polynomial basis functions. The resulting discrete system has the form (2.9). We begin by describing some key implementation issues involved in the numerical experiments.

4.1 Implementation issues

4.1.1 Pressure-splitting scheme

This scheme is used to enhance solving the linear Stokes systems [12] occurring at each stage of an IMEX or DIRK-CF method. Suppose

$$\begin{aligned} \frac{1}{\gamma\Delta t}BY_i - AY_i - D^TZ_i &= B\hat{y}_n \\ DY_i &= 0 \end{aligned} \quad (4.1)$$

represents a linear Stokes system arising from stage i of a first or second order IMEX or DIRK-CF method applied to (2.9), where γ is a parameter of the method. Here the variable \hat{y}_n incorporates the explicit treatment of the convection, the initial data and vector fields at earlier stages. The splitting scheme (irrespective of boundary conditions) is done in the following steps:

$$\text{Step 1: } \frac{1}{\gamma\Delta t}B\hat{Y}_i - A\hat{Y}_i - D^T p_n = B\hat{y}_n$$

$$\text{Step 2: } D^T B^{-1} D \delta p_i = -\frac{1}{\gamma\Delta t} D\hat{Y}_i$$

$$\text{Step 3: } Y_i = \hat{Y}_i - \gamma\Delta t B^{-1} D^T \delta p_i, \quad Z_i = p_n + \delta p_i.$$

Step 1 is an explicit approximation of the stage value of the velocity using the initial pressure. This approximation is not divergence-free. Step 2 and 3 are thus the projection steps which enforce the divergence-free constraint and correct the velocity and pressure. Note that this approximation introduces a truncation error of order 3, and is thus sufficient for methods order upto 2 (see e.g.[12]). Solving (4.1) directly would lead to solving equations with the operator $D^T H D$ (with $H := \frac{1}{\gamma\Delta t}B + A$) for the pressure. However, the cost of inverting $D^T H^{-1} D$ is much higher than for inverting $D^T B^{-1} D$ in Step 2, since B is usually diagonal or tridiagonal an easier to invert than H . This explains the main advantage for using the pressure-splitting schemes in the numerical computations. We have exploited this advantage in the numerical experiments in sections 4.4 and 4.5.

4.1.2 Boundary conditions

We illustrate the strategy for implementing the boundary conditions in the context of spectral element methods. Let R_p represent a periodic boundary operator, defined such that for a given vector y in the solution space or space of vector fields, $R_p y$ is periodic. Each stage of an IMEX or DIRK-CF method applied to (2.9) can be expressed in the form (4.1). Multiplying the first equation of (4.1) by R_p we obtain the system

$$\begin{aligned} HY_i - R_p D^T Z_i &= R_p B\hat{y}_n \\ DY_i &= 0 \end{aligned} \quad (4.2)$$

where $H := R_p(\frac{1}{\gamma\Delta t}B - A)$. The matrix H results from the discrete Helmholtz operator and is symmetric positive-definite (SPD); the mass B is diagonal and SPD, and thus easy to invert. The entire system (4.2) forms a symmetric saddle system, which has a unique solution for Y_i provided D is of full rank. The choice of spatial discretization method provides a full-rank matrix D . The system (4.2) can be solved by a Schur-complement approach and the pressure-splitting scheme.

The treatment of Dirichlet boundary conditions is very similar and we refer to [12] for further details. In the experiments reported in this paper, no special treatment has been taken to enforce pressure boundary conditions, since the discrete pressure space is not explicitly defined on discretization nodes on the boundary.

4.2 Temporal order tests for the IMEX methods

We investigate numerically the temporal order of convergence of some IMEX-RK methods as described in section 3.1. The methods considered here are the second and third order IMEX-RK schemes with stiffly-accurate and L-stable DIRK parts [1]. We refer to them as IMEX2L and IMEX3L respectively. They are given by the Butcher tableaus in Tables 1 and 2 where $\gamma = (2 - \sqrt{2})/2$ and $\delta = 1 - 1/(2\gamma)$.

Table 1: IMEX2L: $\gamma = (2 - \sqrt{2})/2$ and $\delta = 1 - 1/(2\gamma)$

0	0
γ	γ
1	$1 - \gamma$ γ
	$1 - \gamma$ γ

0	0
γ	γ
1	δ $1 - \delta$
	δ $1 - \delta$ 0

Table 2: IMEX3L

$\frac{1}{2}$	$\frac{1}{2}$	0	$\frac{1}{2}$	0
$\frac{2}{3}$	$\frac{1}{6}$	$\frac{1}{2}$	$\frac{11}{18}$	$\frac{1}{18}$
$\frac{1}{2}$	$-\frac{1}{2}$	$\frac{1}{2}$	$\frac{5}{6}$	$-\frac{5}{6}$
1	$\frac{3}{2}$	$-\frac{3}{2}$	$\frac{1}{2}$	$\frac{1}{2}$
	$\frac{3}{2}$	$-\frac{3}{2}$	$\frac{1}{2}$	$\frac{1}{2}$

$\frac{1}{2}$	$\frac{1}{2}$	0	$\frac{1}{2}$	0
$\frac{2}{3}$	$\frac{5}{6}$	$-\frac{5}{6}$	$\frac{1}{2}$	0
$\frac{1}{2}$	$\frac{1}{4}$	$\frac{7}{4}$	$\frac{3}{4}$	$-\frac{7}{4}$
	$\frac{1}{4}$	$\frac{7}{4}$	$\frac{3}{4}$	$-\frac{7}{4}$
		0		

In the first example we consider the Taylor vortex problem with exact solution and initial data given by

$$\begin{cases} u_1 &= -\cos(\pi x_1) \sin(\pi x_2) \exp(-2\pi^2 t/Re), \\ u_2 &= \sin(\pi x_1) \cos(\pi x_2) \exp(-2\pi^2 t/Re), \\ p &= -\frac{1}{4}[\cos(2\pi x_1) + \cos(2\pi x_2)] \exp(-4\pi^2 t/Re), \end{cases} \quad (4.3)$$

writing $Re = 1/\nu$ for the Reynolds number, and $\mathbf{u} := (u_1, u_2)$, $\mathbf{x} := (x_1, x_2)$. The boundary condition is doubly-periodic on the domain $x_1, x_2 \in [-1, 1]$, and we choose $Re = 2\pi^2$. For the spatial discretization we use a spectral method of order $N = 12$, and the time integration is done up to time $T = 1$. For each stepsize $\Delta t = T/2^k$, $k = 1, \dots, 6$, the error between the numerical solution and the exact PDE solution (at time T) are measured in the L_2 -norm, for both the velocity and pressure. The results for both the IMEX2L and IMEX3L show a temporal convergence of order 2 and 3 respectively (see Figure 1).

Similar experiments are carried out for the test problem [18] with exact solution given by

$$\begin{cases} u_1 &= \pi \sin(2\pi x_2) \sin^2(\pi x_1) \sin t, \\ u_2 &= -\pi \sin(2\pi x_1) \sin^2(\pi x_2) \sin t, \\ p &= \cos(\pi x_1) \sin(\pi x_2) \sin t, \end{cases} \quad (4.4)$$

for $x_1, x_2 \in [0, 1]$ and $t \in [0, T]$, with $T = 1$. A corresponding forcing term is added to (1.1) for a given Reynolds number. In this test case we have used $Re = 100$. Meanwhile the boundary condition is homogeneous Dirichlet. The results are shown in Figure 2

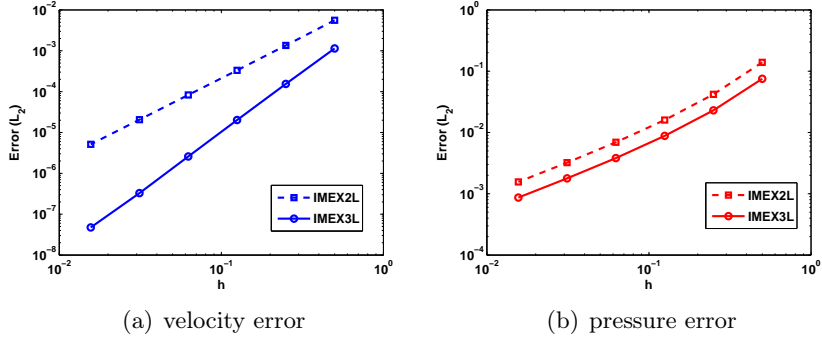


Figure 1: Order of convergence of the IMEX2L and IMEX3L. Test problem: Taylor vortex (4.3); $Re = 2\pi^2$, $T = 1$, $N = 12$, $N_e = 1$, $\Omega = [-1, 1]^2$, $h = \Delta t = T/2^k$, $k = 1, \dots, 6$. bc: periodic. (a) velocity error: IMEX2L (slope = 2.0154), IMEX3L (slope = 2.9250); (b) pressure error: IMEX2L (slope = 1.2773), IMEX3L (slope = 1.2711).

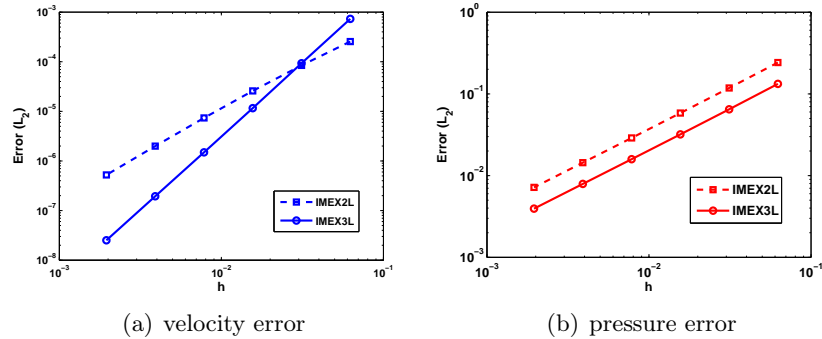


Figure 2: Order of convergence of the IMEX2L and IMEX3L. Test problem:(4.4); $Re = 100$, $T = 1$, $N = 16$, $N_e = 1$, $\Omega = [0, 1]^2$, $h = \Delta t = T/2^k$, $k = 4, \dots, 9$. bc: homogeneous Dirichlet. (a) velocity error: IMEX2L (slope = 1.7908), IMEX3L (slope = 2.9669); (b) pressure error: IMEX2L (slope = 1.0140), IMEX3L (slope = 1.0132).

4.3 Temporal order tests for the DIRK-CF methods

Using the IMEX2L and IMEX3L methods, we construct two DIRK-CF methods, namely, DIRK-CF2L and DIRK-CF3L, of classical orders 2 and 3 respectively. DIRK-CF2L is applied to (2.9) following the algorithm discussed in section 3.2. For DIRK-CF3L we use a similar algorithm at each stage, but an extra update stage added, followed by a projection step to enforce the divergence-free condition. We obtain second order for DIRK-CF2L, but DIRK-CF3L suffer a loss in order (see Figure 3). The flows of the convecting vector fields are computed in a semi-Lagrangian fashion. We believe that the implementation of the boundary conditions alongside the projections is still not very clear from a numerical point of view. The test problem used is the Taylor vortex problem (4.3) with doubly-periodic domain $x_1, x_2 \in [-1, 1]$, and we choose $Re = 2\pi^2$. For the spatial discretization we use a spectral method of order $N = 12$, and the time integration is done up to time $T = 1$. For each stepsize $\Delta t = T/2^k$, $k = 4, \dots, 9$, the velocity error between the numerical solution and the exact PDE solution (at time T) is measured in the L_2 -norm. Meanwhile the pressure error shows first order order of convergence (see Figure 3b).

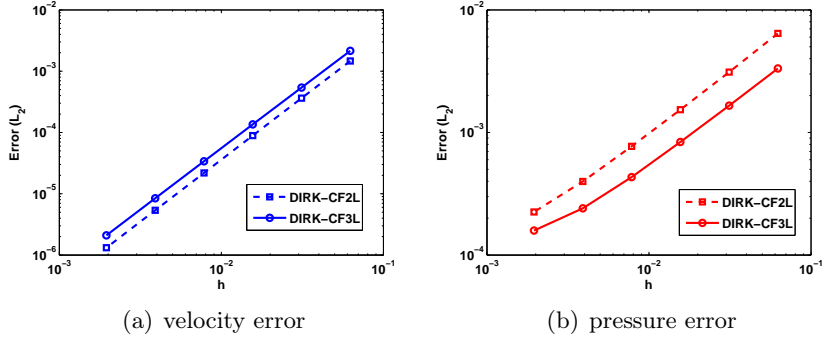


Figure 3: Order of convergence of the DIRK-CF2L and DIRK-CF3L. Test problem: Taylor vortex (4.3); $Re = 2\pi^2$, $T = 1$, $N = 12$, $N_e = 1$, $\Omega = [-1, 1]^2$, $h = \Delta t = T/2^k$, $k = 4, \dots, 9$. bc: periodic. (a) velocity error: DIRK-CF2L (slope = 2.0243), DIRK-CF3L (slope = 2.0000); (b) pressure error: DIRK-CF2L (slope = 0.9734), DIRK-CF3L (slope = 0.8919).

The numerical experiments presented in sections 4.4 and 4.5 illustrate the potentials of the semi-Lagrangian exponential integrators [7] for the treatment of convection-dominated problems. We consider two examples involving high Reynolds incompressible Navier-Stokes models. These examples are the shear-layer rollup problem [4, 11, 13], and the 2D lid-driven cavity problem (see [16, 5] and references therein). The second order semi-Lagrangian DIRK-CF2L method (named SL2L in [7]) is used in each of these experiments. The pressure-splitting technique [12] (discussed in section 4.1.1) is applied to solve the discrete linear Stokes system that arises at each stage of the DIRK-CF method. The semi-Lagrangian schemes associated to the DIRK-CF method are achieved by tracking characteristics and interpolating as in [15].

The results reported in both sections 4.4 and 4.5 indicate that the semi-Lagrangian exponential integrators permit the use of large time stepsizes and Courant numbers.

4.4 Lid-driven cavity flow in 2D

We consider the 2D lid-driven cavity problem on a domain $(x, y) \in \Omega := [0, 1]^2$ with initial data $\mathbf{u} = (u, v) = (0, 0)$ and constant Dirichlet boundary conditions

$$u = \begin{cases} 1 & \text{on upper portion of } \partial\Omega \\ 0 & \text{elsewhere on } \partial\Omega \end{cases}, \quad v = 0 \text{ on } \partial\Omega. \quad (4.5)$$

In Figure 4 we demonstrate the performance of the second order DIRK-CF method (SL2L, by the nomenclature of [7]). Spectral element method (see [13]) on a unit square domain $[0, 1]^2$ with $N_e = 10 \times 10$ uniform rectangular elements and polynomial degree $p = 10$ is used. The specified Reynolds numbers considered are $Re = 400, 3200$. A constant time stepsize, $\Delta t = 0.03$, is used, corresponding to a Courant number of $Cr \approx 9.0911$. In Figure 4c-d we plot the streamline contours of the stream functions, choosing contour levels as in [5]. Meanwhile in Figures 4a-b plots of the centerline velocities (continuous line, for $Re = 400$, dashed line, for $Re = 3200$) show a good match with those reported in [16] (plotted in red circles). The results in Figure 5 show the evolution of the center velocity (at $Re = 400$) up to steady state. It can be observed from this figure that steady state is attained at time $t \approx 40$. At steady state the relative error (L_2 -norm) between the velocity

at a given time and the velocity at the preceding time has decreased to $\mathcal{O}(10^{-8})$. The results also match with those of [23].

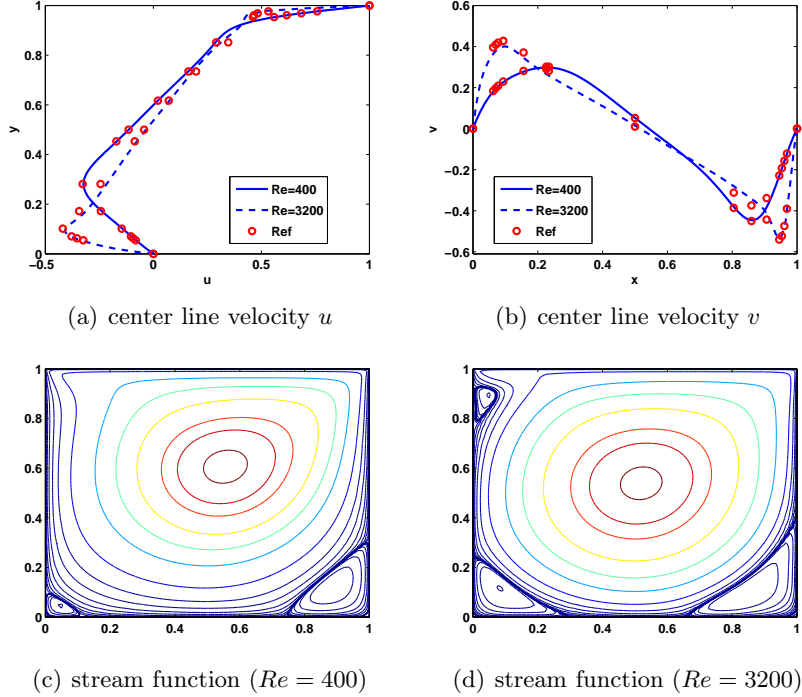


Figure 4: Results of a second order DIRK-CF method for the 2D lid-driven cavity problem. We have $(x, y) \in [0, 1]^2$; $N_e = 10 \times 10$, $N = 10$, $\Delta t = 0.03$, $Cr = 9.0911$. In blue continuous line (our numerical solution); in red circles (\circ , reference solution [16]). (a) Horizontal velocity component u along the vertical center line ($x = 0.5$), (b) Vertical velocity component v along the horizontal center line ($y = 0.5$), (c) Streamline contours of the solution for $Re = 400$, (d) Streamline contours of the solution for $Re = 3200$.

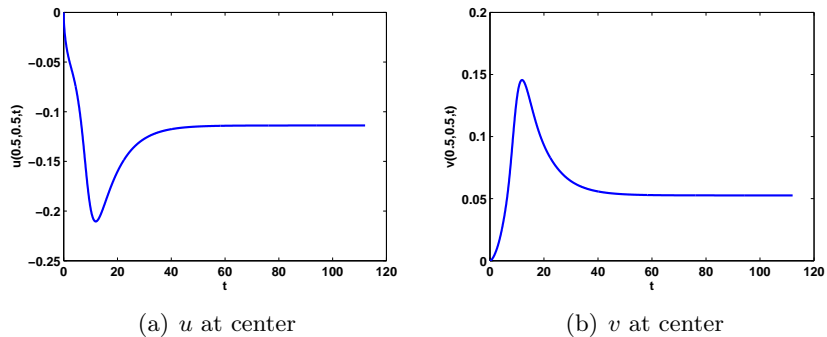


Figure 5: Results of a second order DIRK-CF method for the 2D lid-driven cavity problem. We have $(x, y) \in [0, 1]^2$; $N_e = 10 \times 10$, $p = 10$, $\Delta t = 0.03$, $Cr = 9.0911$, $Re = 400$. (a) Evolution of the horizontal velocity component u at the domain center ($x = 0.5, y = 0.5$): $t \in (0, 112.08)$, (b) Evolution of the vertical velocity component v at the domain center ($x = 0.5, y = 0.5$): $t \in (0, 112.08)$.

4.5 Shear-layer roll up problem

We now consider the shear-layer problem [4, 11, 13] on a domain $\Omega := [0, 1]^2$ with initial data $\mathbf{u} = (u, v)$ given by

$$\begin{cases} \tanh(\rho(y - 0.25)) & \text{for } y \leq 0.5 \\ \tanh(\rho(0.75 - y)) & \text{for } y > 0.5 \end{cases}, \quad v = 0.05 \sin(2\pi x) \quad (4.6)$$

which corresponds to a layer of thickness $\mathcal{O}(1/\rho)$. Doubly-periodic boundary conditions are applied.

In Figure 6 we demonstrate the performance of various second order methods including two DIRK-CF methods (SL2 & SL2L, by the nomenclature of [7]) and a second order semi-Lagrangian multistep exponential integrator (named BDF2-CF2, in [8]). The results are obtained at time $t = 1.5$, using a *filter-based* spectral element method (see [13]) with $N_e = 16 \times 16$ elements and polynomial degree $N = 8$. The specified Reynolds number is $Re = 10^5$, while $\rho = 30$ and time stepsizes used are $\Delta t = 0.002, 0.005, 0.01$ corresponding to a Courant numbers of $Cr \approx 0.6393, 1.5981, 3.1963$ respectively. The filtering parameter used in each experiment is $\alpha = 0.3$ (see for example [13]). However, the time stepsize and Courant number are upto about 10 times larger than that report in [13]. The initial values for the BDF2-CF are computed accurately using the second order DIRK-CF (SL2L) with smaller steps. The results are qualitatively comparable with those in [11, 13].

In Figure 7 we demonstrate the performance of the second order DIRK-CF method (SL2L). The results are obtained at times $t = 0.8, 1.0, 1.2$ and 1.5 respectively, using spectral element method (without filtering) with $N_e = 16 \times 16$ elements and polynomial degree $N = 16$. The specified Reynolds number is $Re = 10^5$, while $\rho = 30$. The time stepsize used is $\Delta t = 0.01$, corresponding to a Courant number of $Cr \approx 11.9250$. This time stepsize is 10 times larger than that report in [13]. Again the results are well comparable to those in [11, 13].

Finally in Figure 8 we demonstrate the performance of the second order DIRK-CF method (SL2L) for the “thin” shear-layer rollup problem, so defined for $\rho = 100$. The results are obtained at times $t = 0.8, 1.0, 1.2$ and 1.5 respectively, using spectral element method (without filtering) with $N_e = 16 \times 16$ elements and polynomial degree $N = 16$. The specified Reynolds number is $Re = 40,000$. The time stepsize used is $\Delta t = 0.01$, corresponding to a Courant number of $Cr \approx 11.9250$. The results are well comparable to those in [11, 13], except that we used 10 times the stepsize in time.

5 Conclusion

We have derived projection methods based on IMEX Runge-Kutta schemes and semi-Lagrangian exponential integrators (DIRK-CF) for the incompressible Navier-Stokes equations. These methods have been shown to perform well in the case of periodic and no-slip boundary conditions. Using model problems in 2D with high Reynolds number, we have demonstrated the performance of the DIRK-CF methods for convection dominated problems. The IMEX methods show upto third order of convergence in the velocity. However, the DIRK-CF methods only show upto second order. Proper ways of implementing the projections alongside the boundary conditions for the DIRK-CF methods are still to be investigated further. We believe this would help recover the full order of the methods.

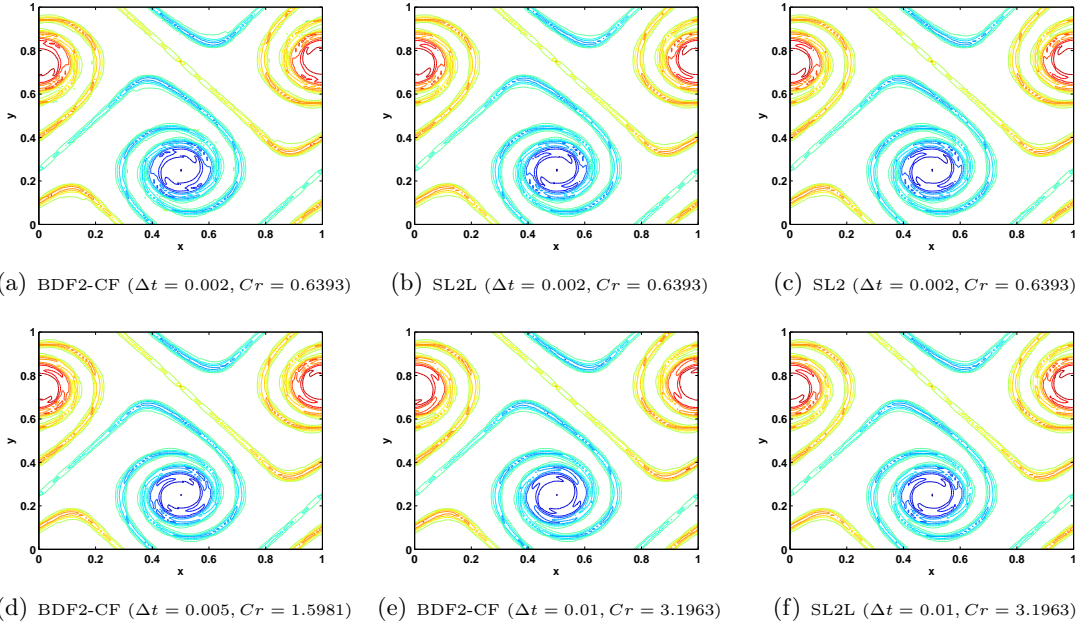


Figure 6: Results of second order DIRK-CF methods (SL2 & SL2L) and BDF2-CF method for the shear-layer rollup problem. We have $(x, y) \in [0, 1]^2$; $N_e = 16 \times 16$, $N = 8$. (filtering, $\alpha = 0.3$), $\rho = 30$, $Re = 10^5$. Vorticity contours (-70 to 70 by 15) of the solution at time $t = 1.5$.

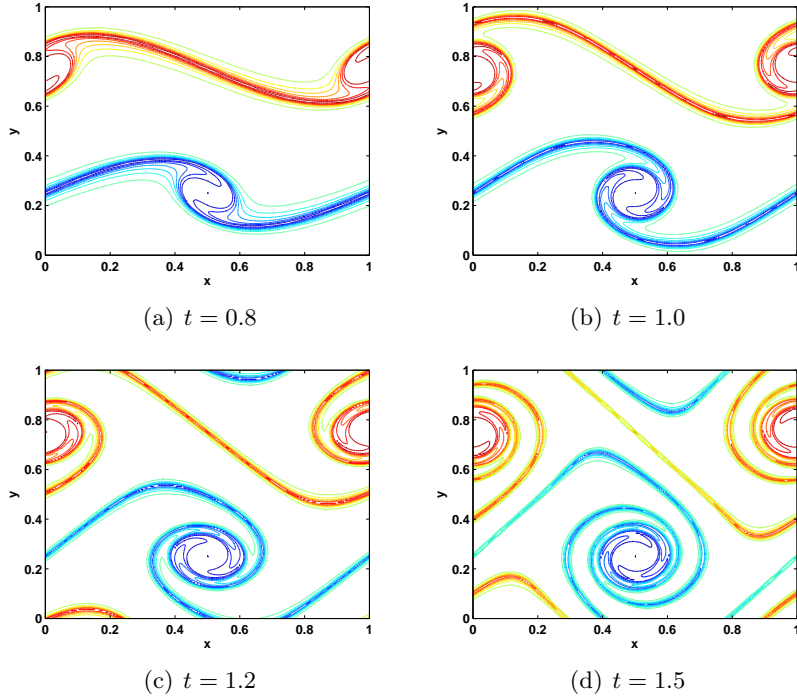


Figure 7: Results of second order DIRK-CF method (SL2L) for the shear-layer rollup problem. We have $(x, y) \in [0, 1]^2$; $N_e = 16 \times 16$, $p = 16$, $\Delta t = 0.01$, $Cr = 11.9250$, $\rho = 30$, $Re = 10^5$. Vorticity contours (-70 to 70 by 15) of the solution at time (a) $t = 0.8$, (b) $t = 1.0$, (c) $t = 1.2$, (d) $t = 1.5$.

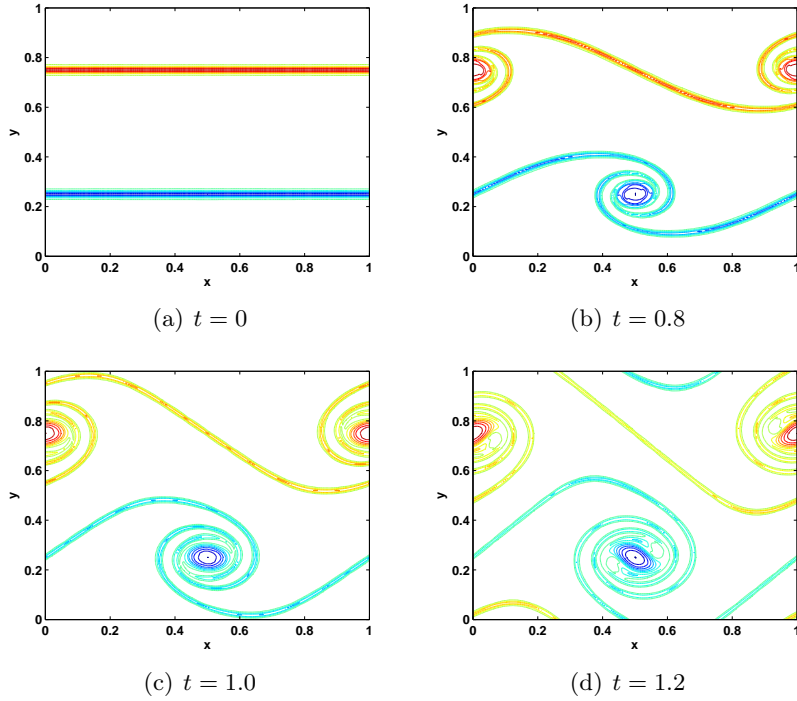


Figure 8: Results of second order DIRK-CF method (SL2L) for the “thin” shear-layer rollup problem. We have $(x, y) \in [0, 1]^2$; $N_e = 16 \times 16$, $p = 16$, $\Delta t = 0.01$, $Cr = 11.9250$. (**no filtering**), $\rho = 100$, $Re = 40,000$. Vorticity contours (-36 to 36 by 13) of the solution at time (a) $t = 0$, (b) $t = 0.8$, (c) $t = 1.0$, (d) $t = 1.2$.

References

- [1] U. M. Ascher, S. J. Ruuth, and R. J. Spiteri, *Implicit-explicit Runge-Kutta methods for time-dependent partial differential equations*, Appl. Numer. Math. **25** (1997), 151–167.
- [2] U. M. Ascher, S. J. Ruuth, and B. T. R. Wetton, *Implicit-explicit methods for time-dependent partial differential equations*, SIAM J. Numer. Anal. **32** (1995), no. 3, 797–823.
- [3] D. L. Brown, R. Cortez, and M. L. Minion, *Accurate projection methods for the incompressible Navier-Stokes equations*, J. Comput. Phys. **168** (2001), no. 2, 464–499. MR 1826523 (2002a:76112)
- [4] D. L. Brown and M. L. Minion, *Performance of under-resolved two-dimensional incompressible flow simulations*, J. Comput. Phys. **122** (1995), no. 1, 165–183. MR 1358529 (96g:76038)
- [5] C.-H. Bruneau and M. Saad, *The 2d lid-driven cavity problem revisited*, Computers & Fluids **35** (2006), no. 3, 326–348.
- [6] E. Celledoni, *Eulerian and semi-Lagrangian commutator-free exponential integrators*, CRM Proceedings and Lecture Notes **39** (2005), 77–90.
- [7] E. Celledoni and B. K. Kormeta, *Semi-Lagrangian Runge-Kutta exponential integrators for convection dominated problems*, J. Sci. Comput. **41** (2009), no. 1, 139–164.

- [8] ———, *Semi-Lagrangian multistep exponential integrators for index 2 differential-algebraic systems*, J. Comput. Phys. **230** (2011), no. 9, 3413–3429. MR 2780470
- [9] A. J. Chorin, *Numerical solution of the Navier-Stokes equations*, Math. Comp. **22** (1968), 745–762. MR 0242392 (39 #3723)
- [10] A. J. Chorin, *On the convergence of discrete approximations to the Navier-Stokes equations*, Math. Comp. **23** (1969), 341–353. MR 0242393 (39 #3724)
- [11] P. Fischer and J. Mullen, *Filter-based stabilization of spectral element methods*, C. R. Acad. Sci. Paris Sér. I Math. **332** (2001), no. 3, 265–270. MR 1817374 (2001m:65129)
- [12] P. F. Fischer, *An overlapping Schwarz method for spectral element solution of the incompressible Navier-Stokes equations*, J. Comput. Phys. **133** (1997), no. 1, 84–101. MR 1445173 (97m:76094)
- [13] P. F. Fischer, G. W. Kruse, and F. Loth, *Spectral element method for transitional flows in complex geometries*, J. Sc. Comput. **17** (2002), no. 1–4, 81–98.
- [14] C. Foias, O. Manley, R. Rosa, and R. Temam, *Navier-Stokes equations and turbulence*, Encyclopedia of Mathematics and its Applications, vol. 83, Cambridge University Press, Cambridge, 2001. MR 1855030 (2003a:76001)
- [15] P.F. Fischer F.X. Giraldo, J.B. Perot, *A spectral element semi-lagrangian (SESL) method for the spherical shallow water equations*, J. Comput. Phys. **190**.
- [16] U. Ghia, K. N. Ghia, and C. T. Shin, *High-re solutions for incompressible flow using the navier-stokes equations and a multigrid method*, Journal of Computational Physics **48** (1982), no. 3, 387–411.
- [17] J. L. Guermond, P. Minev, and J. Shen, *An overview of projection methods for incompressible flows*, Comput. Methods Appl. Mech. Engrg. **195** (2006), no. 44–47, 6011–6045. MR 2250931 (2007g:76157)
- [18] J. L. Guermond and J. Shen, *A new class of truly consistent splitting schemes for incompressible flows*, J. Comput. Phys. **192** (2003), no. 1, 262–276. MR 2045709 (2005k:76076)
- [19] G. E. Karniadakis, M. Israeli, and S. A. Orszag, *High-order splitting methods for the incompressible Navier-Stokes equations*, J. Comput. Phys. **97** (1991), no. 2, 414–443.
- [20] R. Rannacher, *On Chorin’s projection method for the incompressible Navier-Stokes equations*, Lecture Notes in Mathematics, vol. 1530, 1991.
- [21] J. Shen, *On error estimates of projection methods for Navier-Stokes equations: first-order schemes*, SIAM J. Numer. Anal. **29** (1992), no. 1, 57–77. MR 1149084 (92m:35213)
- [22] R. Témam, *Sur l’approximation de la solution des équations de Navier-Stokes par la méthode des pas fractionnaires. II*, Arch. Rational Mech. Anal. **33** (1969), 377–385. MR 0244654 (39 #5968)
- [23] D. Xiu and G. E. Karniadakis, *A semi-Lagrangian high-order method for Navier-Stokes equations*, J. Comput. Phys. **172** (2001), no. 2, 658–684. MR 1857617 (2002g:76077)